5th International Conference on Experimental Fluid Mechanics ICEFM 2018 Munich
Munich, Germany, July 2-4, 2018

# The turbulent velocity and temperature field in a heated duct

**Peter Scholz**[1*], **Henrik Rochlitz**[1]

[1] Technische Universitt Braunschweig, Institute of Fluid Mechanics, Braunschweig, Germany

[*] P.Scholz@tu-braunschweig.de

## Abstract

The flow field and the temperature field are studied in a high-aspect ratio duct flow, where the lower wall is heated to enforce a heat flux into the flow medium. The flowfield is studied with PIV methods and the temperature field by means of planar Laser-induced fluorescence (pLIF) based on a ratiometric two-dye approach. The secondary motion in the duct creates a complex distribution of the mean velocity field with strong gradients in the vicinity of the corner vortices. In the center region, on the other hand, the properties of the turbulence (Reynolds stresses and integral scale) are almost constant along the height of the duct. The pLIF-experiments give access to, yet, the averaged temperature field. The thermal boundary layer is thin, but extents well beyond the stagnation region created by the vortex-induced secondary motion.

## 1 Introduction

In many engineering applications the turbulent flow through rectangular ducts is used for cooling purposes. Though the geometry itself is simple, prediction of the cooling performance of such ducts is a challenging task, because in the sharp-edged corners a vortical secondary motion exists, which is rather weak, but has great influence on the momentum and heat exchange.

Properties of the turbulent flow in rectangular ducts have been studied by several authors, e.g., among many others, Launder and Ying (1972) studied square ducts and Melling and Whitelaw (1976) rectangular ones. Since the most important engineering application of such duct flows is the use as cooling channels, also many studies exist with a heat flux applied to the flow. E.g. Wardana et al. (1994) study the turbulent structures in a rectangular duct of aspect ratio 2.3, at relatively low Re, though. It is known from such studies that the secondary motion exists due to the interaction of turbulent eddies with the duct corners. When it comes to predictions of such flows, relatively simple RANS-approaches might fail to predict the correct sensitivities, because simple one- or two-equation turbulence models are not able to reproduce the development and/or the preservation of the secondary motion. Consequently, scale-resolving approaches must be chosen to study the flow in such ducts, e.g. as published by Vzquez and Mtais (2002), Choi and Park (2013) or Kaller et al. (2017).

Most studies that can be found in literature focus on flows at relatively small *Re*. In contrast, in the use of such flows for cooling purposes the Reynolds number might be chosen relatively large, because the cooling effect would generally be expected to increase with increasing *Re*. It is therefore interesting to contribute experimental studies of cooling duct flows at larger Reynolds numbers.

## 2 Experimental Setup

### 2.1 High aspect-ratio duct flow test bench

The general experimental setup is shown in Fig. 1: Standard tap water is used as a flow medium, it is fed into the test section through a flow straightener, to break up any larger scale vortical components. To ensure an established, turbulent flow state, the water flows through an isothermal feed line with the same nominal cross section as the test section itself. The heated region starts 660 mm downstream of the straightener and is 600 mm long. The field of view is 375 mm downstream of the begin of the heated region. After having

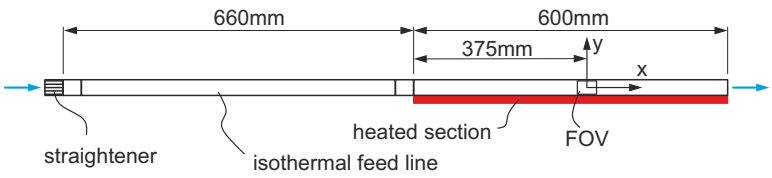


Figure 1: Sketch of the experimental layout

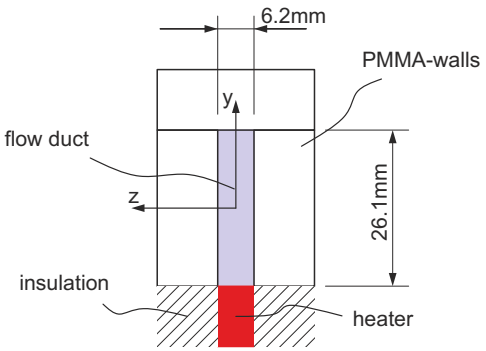


Figure 2: Cross section of the heated test section

passed the test section, the water runs into a collection tank. A pump sucks the water from that tank through a flow meter and supplies it to the intake to close the loop.

Fig. 2 shows details of the test section. Both sidewalls and the upper wall are made of transparent PMMA to provide optical access. In fact, the upper wall at the position of the field of view (FoV) is manufactured as a removable hatch, to allow installation of a calibration plate. The section itself is $w = 6.23\,\text{mm}$ wide with a height of $h = 26.1\,\text{mm}$, giving an aspect ratio of 4.2 and a hydraulic diameter of $d_h = 10.06\,\text{mm}$. Herein, we focus on the center section of the duct, i.e. $z = 0\,\text{mm}$ at the position $x$ indicated above.

The lower wall of the test section can be heated. A large copper block with a tapered tip is equipped with cartridge heaters with a total electric power of 14 kW. The upper, thin end of this block is taken as the lower wall of the test section. The PMMA-sidewalls are insulated from the heated block by inlays made of a thermoplastic polymer (PEEK), such that the side walls can be considered adiabatic and the heat flux into the flow is solely supplied through the lower wall.

In the following we will focus on a test case with a total flow rate of $\dot{V} = 50\,\text{l/min}$. The nominal bulk velocity is $u_b := \dot{V}/(b \cdot h) = 5.12\,\text{m/s}$. A second cooling/heating system in the collection tank conditions the water to a bulk temperature of $T_b = 60\,^\circ\text{C}$, which gives $Re = 110\,000$ (based on hydraulic diameter). The lower wall (i.e. the copper block) is heated to $T_W = 100\,^\circ\text{C}$.

## 2.2 PIV system

The flowfield inside the duct was measured using a 3C2D-PIV-System (“Stereo-PIV”), consisting of two LaVision Imager Intense cameras (a.k.a. PCO Sensicam). The cameras are mounted enclosing an angle of approximately 90, with both cameras imaging the FoV through the same side wall. The Laser was mounted on a stand, the lightsheet optics was built with lenses using microbench-components for positioning. The laser-lightsheet entered the test section through the upper wall.

The system was controlled using LaVision’s DaVis 8 control software, which was also used for evaluation of the particle images. 1500 individual snapshots have been acquired and processed for each dataset. Refer to Rochlitz et al. (2015) for more details of the experimental setup of the PIV system.

## 2.3 Planar LIF

The temperature field in the duct was measured using a two-dye, planar, LIF-technique. Two different dyes, namely Rhodamine 110 and Rhodamine B, are solved in the flow medium. Both dyes fluoresce, when excited by a laser of proper wavelength. The same Nd:YAG-Laser (wavelength 532 nm), which is used

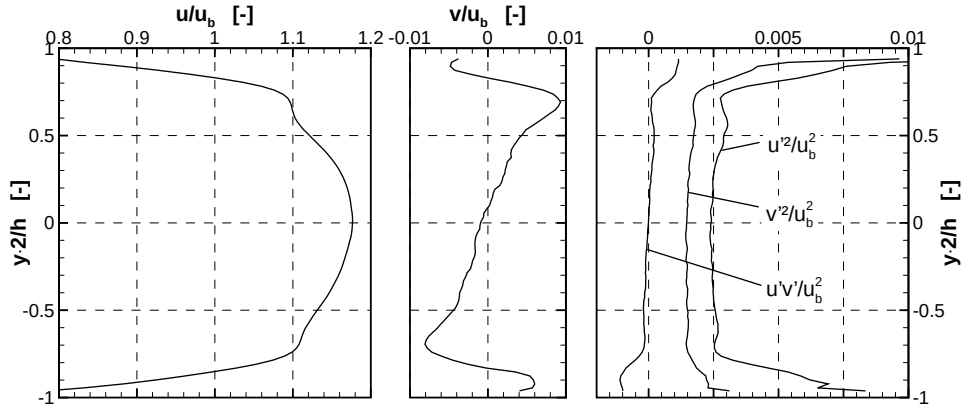


Figure 3: Mean velocities and turbulent stresses

for PIV, was used herein to excite the dyes. Both dyes feature a different sensitivity to temperature: For Rhodamine B the absorption at 532 nm is practically insensitive to temperature, but the quantum efficiency and therefore the fluorescence intensity $I_{RhB}$ decreases with increasing temperature. The quantum efficiency of Rhodamine 110 on the other hand is independent of temperature, but the absorption at 532 nm increases with increasing temperature and so does the fluorescence intensity $I_{Rh110}$. In effect, the ratio of the two fluorescence intensities detected at one point is a function of temperature, but independent of the exact excitation energy.

The system used for the pLIF studies consists of two LaVision Imager Intense cameras, both imaging the same FoV. Again, the Laser was mounted on a stand and equipped with a light sheet optics to excite the dyes in the center plane of the duct. One camera was equipped with a 575 nm optical longpass-filter, to limit the imaging to the fluorescence of the Rhodamine B. The other camera was equipped with a combination of a 550 nm shortpass and a 532 nm notch filter, to record the fluorescence of the Rhodamine 110. Dye concentration, filter combinations and excitation energies have been varied in a comprehensive preliminary study, to find the setup with the best signal-to-noise ratio and the lowest crosstalk between the two signals.

Refer to Rochlitz and Scholz (2018) for more details of the experimental setup of the pLIF-System, particularly regarding dye concentrations and the calibration process.

# 3 Results

## 3.1 Flow field

Time-Averaged results of the PIV measurements are shown in Fig. 3. The data compares well with large-eddy simulations, as was shown by Kaller et al. (2017), though the turbulence level in the experiments seems to be larger than predicted in the simulations. The velocity profiles show a characteristic pattern, where the regions close to the top and bottom wall (in the range $|1| > y \cdot 2/h \approx > |0.5|$) are influenced by secondary vortices residing in the edges of the duct. As can be seen in Kaller et al. (2017), two pairs of counter-rotating vortices exist, one pair at $y \cdot 2/h \approx \pm 0.95$ and one at $y \cdot 2/h \approx \pm 0.75$. These pairs create a stagnation of the secondary motion at $y \cdot 2/h \approx \pm 0.85$, which is clearly visible in the $v/u_b$-distribution.

The flow in the center region of the duct is not significantly influenced by these vortices, with almost constant turbulence properties. Note that the half-width of the duct is $w = h/4.2$ (in dimensionless notation, i.e. the aspect ratio) – in other words, for all regions $|y \cdot 2/h| < 0.76$ the sidewalls of the duct are closer than the lower wall.

The left part Fig. 4 shows two two-point-correlation coefficients of longitudinal velocity $R_{uu}$ in two positions, one in the center section of the duct $y \cdot 2/h = 0$, and one close to the lower wall at $y \cdot 2/h = -0.82$. The right part shows the integral scale of the turbulent structures, based on these correlations. The axis is given relative to the height of the duct and relative to the width. As can be seen, the size of the large-scale turbulent structures is relatively constant in the center of the duct and is similar to half of the width. Near the secondary vortices at approximately $|y \cdot 2/h| < 0.76$, the integral scale becomes significantly smaller.

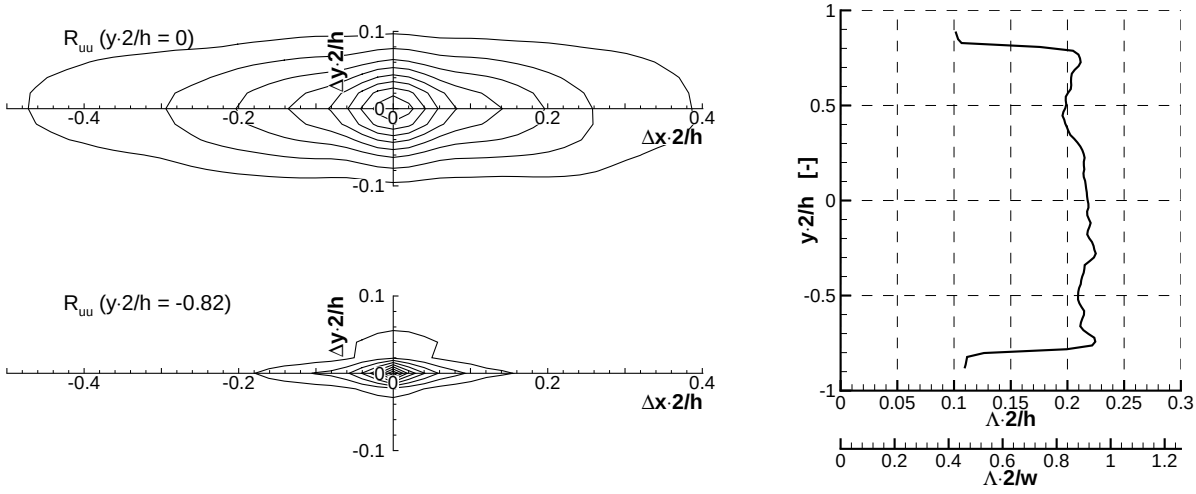


Figure 4: (Left) Two-point cross-correlation coefficient $R_{uu}$ at two points in the duct (contour lines $\Delta R_{uu} = 0.1$, with first line is $R_{uu} = 0.2$; (Right) Integral turbulent scale $\Lambda$ over the duct heigth

### 3.2 Temperature field

Fig. 5 shows the mean temperature profiles in the center section of the duct, near the lower, heated wall. The bulk temperature is $T_b = 60\,^{\circ}\mathrm{C}$ for all cases shown. In the left subfigure, to highlight the sensitivity of the pLIF-measurements, the wall temperature is increased in steps of $\Delta T_W = 10\,^{\circ}\mathrm{C}$, where $T_W = 60\,^{\circ}\mathrm{C}$ is the adiabatic case without any heat transfer. It can be seen how the temperature profile near the wall responds to the different wall temperatures. However, since in this case the effective bulk Reynolds-number is constant, the thickness of the thermal boundary layer stays constant.

In the center subfigure of Fig. 5 the mass flow rate (and bulk velocity $u_b$, and Reynolds-number, respectively) was varied in steps of 12%, while, both, the bulk temperature ($T_b = 60\,^{\circ}\mathrm{C}$) and the wall temperature ($T_W = 100\,^{\circ}\mathrm{C}$) were held constant. Since the Reynolds-number effectively varies in these cases, the thickness of the thermal boundary layer varies, too.

The rightmost subfigure repeats the velocity component $v$ normal to the heated wall in direct comparison to the temperature profiles. As already said, a stagnation point exists at around $y \cdot 2/h \approx 0.82$ due to the vortices in the duct corners. In the lower region the $v$-component of the vortices supports the diffusion of temperature into the bulk flow, whereas in the region above $y \cdot 2/h \approx 0.82$ the vortices are counterproductive for the heat transfer. As can be seen, the temperature boundary layer clearly extents beyond the stagnation area of $v$.

The noise in the temperature distributions is not insignificant, which is due to the high bulk temperature and accompanying small variations of temperature in the field. In this case, only the mean temperature distribution can be acquired, because averaging is required to reduce noise. However, if bulk temperature and/or mass flow rate are reduced, also instantaneous snapshots of the temperature field can be analyzed, as shown in Rochlitz and Scholz (2018). In future experiments effort will be made to increase sensitivity at large bulk temperatures, to give access to temperature fluctuations also at larger Re.

## 4 Conclusion

The contribution presents measurement of the flow- and temperature-field in a rectangular duct. The flow was measured using a Stereo-PIV-system, the temperature field was measured using a planar, two-color, ratiometric LIF-approach. Some data was shown as an example: The velocity field, including the turbulent stresses and integral length scale, and the temperature fields.

The data that can be generated in this faciliy can be used as validation data for numerical simulations and to study the details of the heat transfer mechanisms. To do so, the sensitivity of the pLIF technique must be increased, to have access to instantaneous temperature fields even at these large bulk temperatures and

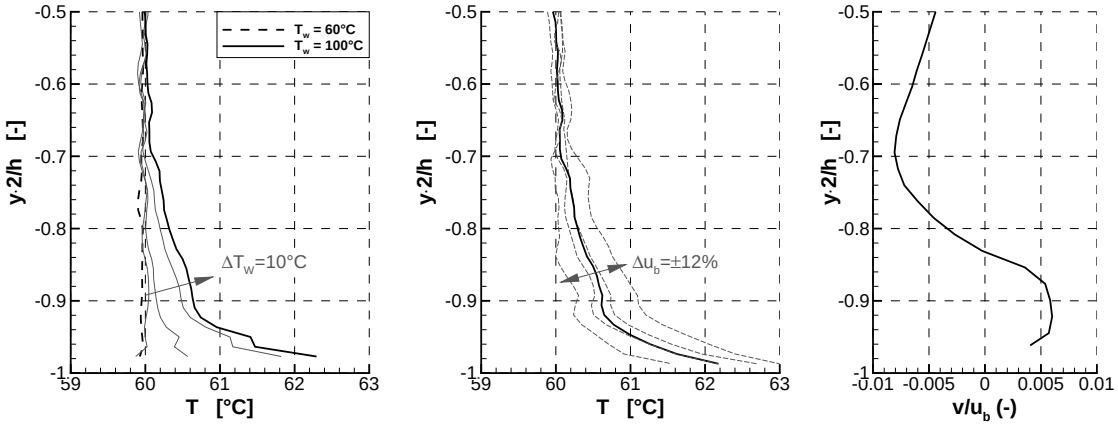


Figure 5: Temperature profiles near the lower, heated wall with (Left) varying wall temperature and (Middle) varying mass flow rate; (Right) Wall-normal velocity, as shown in Fig. 3

flow rates. If this objective has been reached, simultaneous PIV- and pLIF-measurements can be conducted, using one Laser for, both, PIV and LIF, giving access to velocity-temperature-correlations.

## Acknowledgements

The work was funded by the German Research Foundation “Deutsche Forschungsgemeinschaft (DFG)” in the framwork of the Collaborative Research Center “TRR 40”: “Fundamental Technologies for the Development of Future Space-Transport-System Components under High Thermal and Mechanical Loads”

## References

Choi H and Park T (2013) The influence of streamwise vortices on turbulent heat transfer in rectangular ducts with various aspect ratios. *International Journal of Heat and Fluid Flow* 40:1 – 14

Kaller T, Pasquariello V, Hickel S, and Adams NA (2017) Large-eddy simulation of the high-Reynolds-number flow through a high-aspect-ratio cooling duct. 10th International Symposium on Turbulence and Shear Flow Phenomena (TSFP10). chicago, USA

Launder BE and Ying WM (1972) Secondary flows in ducts of square cross-section. *Journal of Fluid Mechanics* 54:289–295

Melling A and Whitelaw JH (1976) Turbulent flow in a rectangular duct. *Journal of Fluid Mechanics* 78:289315

Rochlitz H and Scholz P (2018) Application of laser-induced fluorescence technique in a duct flow with one heated wall. *Experiments in Fluids* 59:54

Rochlitz H, Scholz P, and Fuchs T (2015) The flow field in a high aspect ratio cooling duct with and without one heated wall. *Experiments in Fluids* 56:208

Vzquez MS and Mtais O (2002) Large-eddy simulation of the turbulent flow through a heated square duct. *Journal of Fluid Mechanics* 453:201–238

Wardana ING, Ueda T, and Mizomoto M (1994) Effect of strong wall heating on turbulence statistics of a channel flow. *Experiments in Fluids* 18:87–94